

# Global distributions of water vapour isotopologues retrieved from IMG/ADEOS data

H. Herbin<sup>1</sup>, D. Hurtmans<sup>1</sup>, S. Turquety<sup>2</sup>, C. Wespes<sup>1</sup>, B. Barret<sup>1,\*</sup>, J. Hadji-Lazaro<sup>2</sup>, C. Clerbaux<sup>1,2</sup>, and P.-F. Coheur<sup>1,3</sup>

<sup>1</sup>Spectroscopie de l'Atmosphère, Service de Chimie Quantique et de Photophysique, Université Libre de Bruxelles (U.L.B.), Brussels, Belgium

<sup>2</sup>Service d'Aéronomie/IPSL, CNRS, Université Pierre et Marie Curie, Paris, France

<sup>3</sup>Research Associate with the F.N.R.S, Belgium

\* now at: Laboratoire d'Aérodynamique, UMR 5560 CNRS/Université Paul Sabatier, Observatoire de Midi-Pyrénées, Toulouse, France

Received: 28 February 2007 – Published in Atmos. Chem. Phys. Discuss.: 5 April 2007

Revised: 25 June 2007 – Accepted: 13 July 2007 – Published: 25 July 2007

**Abstract.** The isotopologic composition of water vapour in the atmosphere provides valuable information on many climate, chemical and dynamical processes. The accurate measurements of the water isotopologues by remote-sensing techniques remains a challenge, due to the large spatial and temporal variations. Simultaneous profile retrievals of the main water isotopologues (i.e. H<sub>2</sub><sup>16</sup>O, H<sub>2</sub><sup>18</sup>O and HDO) and their ratios are presented here for the first time, along their retrieved global distributions. The results are obtained by exploiting the high resolution infrared spectra recorded by the Interferometric Monitor for Greenhouse gases (IMG) instrument, which has operated in the nadir geometry onboard the ADEOS satellite between 1996 and 1997. The retrievals are performed on cloud-free radiances, measured during ten days of April 1997, considering two atmospheric windows (1205–1228 cm<sup>-1</sup>; 2004–2032 cm<sup>-1</sup>) and using a line-by-line radiative transfer model and an inversion procedure based on the Optimal Estimation Method (OEM). Characterizations in terms of vertical sensitivity and error budget are provided. We show that a relatively high vertical resolution is achieved for H<sub>2</sub><sup>16</sup>O (~4–5 km), and that the retrieved profiles are in fair agreement with local sonde measurements, at different latitudes. The retrieved global distributions of H<sub>2</sub><sup>16</sup>O, H<sub>2</sub><sup>18</sup>O, HDO and their ratios are presented and found to be consistent with previous experimental studies and models. The Ocean-Continent difference, the latitudinal and vertical dependence of the water vapour amount and the isotopologic depletion are notably well reproduced. Others trends, possibly related to small-scale variations in the vertical profiles are also discussed. Despite the difficulties encountered for computing

accurately the isotopologic ratios, our results demonstrate the ability of infrared nadir sounding for monitoring atmospheric isotopologic water vapour distributions on a global scale.

## 1 Introduction

Water vapour is involved in many key atmospheric processes including radiative transfer, dynamics or homogeneous and heterogeneous chemistry (Solomon, 1999; Coffey et al., 2006). The study of atmospheric water vapour has further gained interest since the discovery of the increasing humidity over the last half century (Rosenlof et al., 2001; 2003), the causes of which are not yet fully understood (Kuang et al., 2003; McCarthy et al., 2004; Franz and Rockmann, 2005; Schmidt et al., 2005; Coffey et al., 2006). In the stratosphere, the amount of water vapour has a direct impact on the concentration of the OH radical, which is involved in catalytic cycles of ozone destruction, chlorine activation, denitrification and methane decomposition (Forster and Shine, 2002; Kirk-Davidoff et al., 1999; Tabazadeh et al., 2000; Shindell, 2001; McCarthy et al., 2004). In the troposphere, water is the principal component of the global climate system: it acts on clouds, precipitations and also plays a role in the greenhouse effect (Schneider et al., 1999; Hartmann, 2002).

The measurement of the isotopologic composition of atmospheric water vapour is used to derive information on the water cycle (Bechtel and Zahn, 2003), paleoclimate (Masson-Delmotte et al., 2005; Jouzel et al., 1997), cloud physics (Webster and Heymsfield, 2003), troposphere-stratosphere exchanges (Kuang et al., 2003; Moyer et al., 1996) and climate studies (precipitations, storms, hurricanes)

Correspondence to: H. Herbin  
(hherbin@ulb.ac.be)

(Bowen and Revenaugh, 2003; Ciais and Jouzel, 2004; Gedzelman et al., 2003; Smith, 1992; Lawrence et al., 2002). This is because isotopologic ratios of water strongly depend upon the evaporation conditions and the condensation history of the air mass during transport (Strong et al., 2007). The process is known as the Vapour Pressure Isotopologue Effect (VPIE): Heavier isotopologues (here HDO and  $\text{H}_2^{18}\text{O}$ ) have lower vapour pressures than the lighter one ( $\text{H}_2^{16}\text{O}$ ) and this leads to an isotopologic fractionation during changes of phase. Hence, when the vapour phase and the condensed phase are in thermodynamic equilibrium, the lighter isotopologues condense more slowly and evaporate at a higher rate than the heavier ones, which in turn concentrate in the liquid or solid phase. The result of this VPIE is that the heavier isotopologic species of atmospheric water are progressively removed and become depleted relative to the Standard Mean Ocean Water (SMOW) values.

An accurate knowledge of the vertical and horizontal distribution of the different water isotopologues is of great interest for a better understanding of the processes controlling the water vapour budget (Bechtel and Zahn, 2003; Worden et al., 2007). However, their quick changes of concentration in space and time, associated with the very important concentration decay with altitude is a difficulty, and few measured profiles of the heavier isotopologues of water vapour have been reported (Zahn et al., 2006, and references therein). The measurements from space-borne instruments, which are the only means for determining extended spatial distributions, are particularly sparse: In previous works, the Atmospheric Trace Molecule Spectroscopy (ATMOS) instrument was used to measure  $\text{H}_2^{16}\text{O}$ , HDO and their ratio in the Upper Troposphere and Lower Stratosphere (UT/LS). It provided information mainly on transport in the tropical UT/LS (Moyer et al., 1996; Kuang et al., 2003). The Interferometric Monitor for Greenhouse gases (IMG) provided a latitudinal distribution of HDO around 4 km (Zakharov et al., 2004). Finally, measurements made with the Tropospheric Emission Spectrometer (TES) have recently enable deriving global distributions of the tropospheric HDO/ $\text{H}_2^{16}\text{O}$  ratio (Worden et al., 2006 and 2007).

In this work, we intend to go further in probing the isotopologic composition of water vapour from satellite. The principal objective of this paper is to characterize the capabilities of high-spectral resolution infrared nadir sounder to provide simultaneous information on the vertical and zonal concentration distributions of three isotopologues ( $\text{H}_2^{16}\text{O}$ ,  $\text{H}_2^{18}\text{O}$  and HDO) and their ratio. For  $\text{H}_2^{18}\text{O}$ , these are the first attempts of retrievals in the nadir view.

In the next section, the IMG instrument, the spectra and the retrieval method are briefly described. Section 3 presents the profiles of the different water isotopologues and their ratio for a small selection of IMG spectra coincident with water balloon-borne soundings. The comparison of the retrieved profiles with sonde data is discussed with respect to the mea-

surement vertical sensitivity and error sources. Section 4 presents the distribution of each isotopologic species and of the isotopologic ratios in partial columns between ground and 16 km of altitude. The quasi-global scale is achieved by analysis the longest IMG operation period, corresponding to ten successive days in April 1997. The spatial variability of HDO/ $\text{H}_2^{16}\text{O}$  and  $\text{H}_2^{18}\text{O}/\text{H}_2^{16}\text{O}$  ratios are presented and discussed based upon the retrieval results. Section 5 summarizes our results and puts forward some perspectives for future applications.

## 2 Measurements and methods

### 2.1 Measurements

The IMG instrument was launched onboard the ADEOS platform on August 1996 and ceased operating in June 1997 (Kobayashi et al., 1999). ADEOS was a sun-synchronous, ground-track repeat polar orbiting satellite at about 800 km altitude, providing a global Earth coverage in 4 days. The IMG instrument was a nadir-viewing Fourier transform interferometer that recorded the thermal infrared emission of the Earth-atmosphere system between 650 and 3000  $\text{cm}^{-1}$ . Its maximum optical path difference was 10 cm, leading to a nominal spectral resolution of 0.1  $\text{cm}^{-1}$ . The spectral range was covered by three separate spectral portions: two photovoltaic InSb detectors were used to record band 1 from 2300 to 3000  $\text{cm}^{-1}$  and band 2 from 2000 to 2500  $\text{cm}^{-1}$ , and a photoconductive type HgCdTe detector was used for band 3 from 600 to 2000  $\text{cm}^{-1}$ . Each detector had a field of view corresponding to a 8 km  $\times$  8 km footprint on the ground and each footprint is separated by a distance of 4 km from the other. The IMG spectra were recorded in batches of six successive measurements, separated by 86 km along the track, followed by reference blackbody calibration measurements. The IMG operation mode was limited to periods of 4 successive days of measurement out of 10 days, except for a single period of ten days from the 1 to 10 April 1997. Due to the very weak signal to noise ratio, the band 1 has not been exploited up to now.

In this study, we use the spectra from 1–10 April 1997 period, provided by bands 2 and 3. The vertical distributions are retrieved from the spectra using the *Atmosphit* software developed at the Université Libre de Bruxelles. This software is based on a detailed line-by-line radiative transfer model, including ray tracing for various geometries and a retrieval scheme that relies on the Optimal Estimation Method (OEM) (Rodgers, 2000). The theoretical elements relevant for the present study are similar to those described by Barret et al. (2005) and Coheur et al. (2005). They are only briefly summarized hereafter.



## 2.2 Retrieval methodology

For an atmosphere divided in discrete layers, the forward radiative transfer equation gives an analytical relationship between the measured vector  $\mathbf{y}$  (in our case, the radiance) and the true atmospheric state  $\mathbf{x}$  (variables to be retrieved: surface temperature, vertical concentration profile, *etc*) and is written as:

$$\mathbf{y} = \mathbf{F}(\mathbf{x}; \mathbf{b}) + \varepsilon \quad (1)$$

where  $\mathbf{F}$  is the forward radiative transfer function,  $\mathbf{b}$  represents the fixed parameters affecting the measurement (atmospheric temperature, pressure, instrumental line shape (ILS), *etc.*) and  $\varepsilon$  is the measurement noise.

A synthetic spectrum, approximation of  $\mathbf{F}$ , is computed using the line parameters (positions, intensities, broadening, shifting and their temperature dependency) and absorption cross-sections compiled in spectroscopic databases, as well as the absorption continua from the MT-CKD model (Clough et al., 2005). The molecular absorption lines are computed using a Voigt line shape and the resulting spectrum is processed to account for the ILS contribution.

The retrieval method aims at determining the state vector  $\mathbf{x}$  from the measurement vector  $\mathbf{y}$ . For nadir-viewing satellites, however, the spectra provide an integrated view of the atmosphere. As a consequence, the retrieval of a vertically resolved profile from the measurement is mathematically ill conditioned, meaning that it has no unique solution. A meaningful solution can, however, be obtained by regularizing the retrieval with a priori information about the variables. This information is composed of an a priori profile  $\mathbf{x}_a$  and an a priori variance-covariance matrix  $\mathbf{S}_a$  (Rodgers, 2000). In this case, the goal of the inversion is to find  $\hat{\mathbf{x}}$ , which is the approximation of the true state  $\mathbf{x}$ , which best agrees with both the measurement and the a priori information.  $\hat{\mathbf{x}}$  is found by iterating:

$$\hat{\mathbf{x}}_{i+1} = \mathbf{x}_a + (\mathbf{K}_i^T \mathbf{S}_\varepsilon^{-1} \mathbf{K}_i + \mathbf{S}_a^{-1})^{-1} \mathbf{K}_i^T \mathbf{S}_\varepsilon^{-1} [\mathbf{y} - \mathbf{F}(\hat{\mathbf{x}}_i) + \mathbf{K}_i(\hat{\mathbf{x}}_i - \mathbf{x}_a)], \quad (2)$$

with  $\mathbf{K}$  being the Jacobian matrix, the rows of which are the partial derivatives of the measurement with respect to the retrieved variables:  $\mathbf{K} = \partial \mathbf{y} / \partial \mathbf{x}$ .  $\mathbf{S}_\varepsilon$  is the measured signal error variance-covariance matrix and is chosen to be diagonal with identical diagonal elements  $\sigma_\varepsilon^2$  ( $\mathbf{S}_\varepsilon = \sigma_\varepsilon^2 \mathbf{I}$ ) (Barret et al., 2005; Coheur et al., 2005), where  $\sigma_\varepsilon$  is a constraint representing the noise equivalent spectral radiance. The retrieved state is obtained after convergence, when the absolute difference between every element of  $\mathbf{F}$  modeled at two successive iteration steps,  $|\mathbf{F}(\hat{\mathbf{x}}_{i+1}) - \mathbf{F}(\hat{\mathbf{x}}_i)|$ , is less than a fraction (20%) of  $\sigma_\varepsilon$ .

The characterization of the retrieved quantities in terms of sensitivity and error sources is essential to estimate the quality of the results. In the case of the linear approximation used

here, the OEM provides an efficient way for characterizing the retrieved state, which is given by (Rodgers, 2000):

$$\hat{\mathbf{x}} = \mathbf{x}_a + \mathbf{A}(\mathbf{x} - \mathbf{x}_a) + \mathbf{G}(\varepsilon + \mathbf{K}_b(\mathbf{b} - \hat{\mathbf{b}})), \quad (3)$$

where  $\hat{\mathbf{b}}$  is the approximate of the model parameters  $\mathbf{b}$ , the Jacobian  $\mathbf{K}_b = \partial \mathbf{F} / \partial \mathbf{b}$  characterizes the sensitivity of the forward model  $\mathbf{F}$  to the model parameters.  $\mathbf{G}$  is the gain matrix whose rows are the derivatives of the retrieved state with respect to the spectral points and it is defined by:

$$\mathbf{G} = \partial \hat{\mathbf{x}} / \partial \mathbf{y} \quad (4)$$

$\mathbf{A}$ , the averaging kernel matrix, gives a measure of the sensitivity of the retrieved state to the true state. It is defined by:

$$\mathbf{A} = \partial \hat{\mathbf{x}} / \partial \mathbf{x} = \mathbf{GK} \quad (5)$$

At a given level, the peak of the averaging kernel row gives the altitude of maximum sensitivity whereas its full width at half maximum is an estimate of the vertical resolution. The trace of  $\mathbf{A}$ , known as the Degrees Of Freedom for Signal (DOFS), indicates the number of independent values of the state vector which can be retrieved from the measurements.

The global error can be inferred from Eq. (3) by considering the difference between the retrieved and the true state:

$$\hat{\mathbf{x}} - \mathbf{x} = (\mathbf{A} - \mathbf{I})(\mathbf{x} - \mathbf{x}_a) + \mathbf{G}\varepsilon + \mathbf{GK}_b(\mathbf{b} - \hat{\mathbf{b}}) \quad (6)$$

This Eq. (6) can be decomposed into three different contributions:

- $(\mathbf{A} - \mathbf{I})(\mathbf{x} - \mathbf{x}_a)$  is the smoothing error, which accounts for the vertical sensitivity of the measurements to the retrieved profile.

- $\mathbf{G}\varepsilon$  is the measurement error, associated to the spectral noise.

- $\mathbf{GK}_b(\mathbf{b} - \hat{\mathbf{b}})$  is the model parameters error, which represents the imperfect knowledge of the model parameters.

Their covariances matrices are respectively given by:

$$\mathbf{S}_{\text{smoothing}} = (\mathbf{A} - \mathbf{I})\mathbf{S}_a(\mathbf{A} - \mathbf{I})^T \quad (7)$$

$$\mathbf{S}_{\text{meas.}} = \mathbf{G}\mathbf{S}_\varepsilon\mathbf{G}^T \quad (8)$$

$$\mathbf{S}_{\text{mod.param.}} = \mathbf{GK}_b\mathbf{S}_b(\mathbf{GK}_b)^T \quad (9)$$

with  $\mathbf{S}_b$  representing uncertainty on the forward model parameters. The latter includes the impact of interfering species, which are simultaneously fitted, as well as the uncertainty on the air temperature profile (uncorrelated uncertainty of 5 K on each retrieved level). We use the same ILS as in previous studies (Barret et al., 2005 and Coheur et al., 2005) and the HITRAN line parameters error is not considerate.

The total error variance-covariance matrix can then be regarded as the sum of these individual contributions:

$$\mathbf{S}_{\text{total}} = \mathbf{S}_{\text{smoothing}} + \mathbf{S}_{\text{meas.}} + \mathbf{S}_{\text{mod.param.}} \quad (10)$$

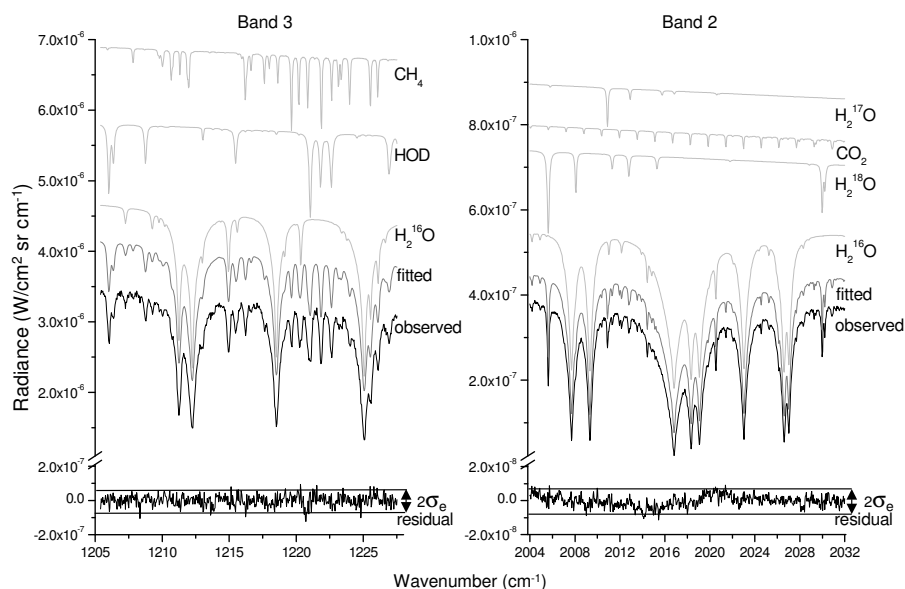


**Fig. 1.** Spectral windows used for retrieving  $\text{H}_2^{16}\text{O}$ ,  $\text{H}_2^{18}\text{O}$  and HDO profiles. Top and middle: IMG radiance spectra and principal individual contributions of the main absorbers in the IMG band 2 and band 3 spectral ranges. Bottom: Residuals (observed-calculated spectra), plotted with an expanded scale and compared to the  $\sigma_\varepsilon$  value.

### 2.3 Data analysis

For the retrievals, the a priori state vector  $\mathbf{x}_a$ , the a priori covariance matrix  $\mathbf{S}_a$ , and additional input parameters, including the pressure and the temperature profiles, have been built based on data from the European Center for Medium Range Weather Forecasts (ECMWF). The a priori information used, for water vapour, associated with the IMG period analyzed here, comes from a latitudinal set ( $+90^\circ$ ,  $+60^\circ$ ), ( $+60^\circ$ ,  $+23^\circ$ ), ( $+23^\circ$ ,  $-23^\circ$ ), ( $-23^\circ$ ,  $-60^\circ$ ) and ( $-60^\circ$ ,  $-90^\circ$ ) of profiles averaged over the months March to May, for 3 successive years (1995, 1996, 1997). It covers altitudes ranging from the ground to 44 km by step of 2 km. The a priori constraint vector and covariance matrices for HDO and  $\text{H}_2^{18}\text{O}$  are identical to those of  $\text{H}_2^{16}\text{O}$  but multiplied by the standard isotopologic ratio. The spectroscopic parameters were extracted from the HITRAN 2004 database (Rothman et al., 2005). The noise equivalent spectral radiance  $\sigma_\varepsilon$  of the IMG instrument was estimated to be of the order of  $2 \times 10^{-9} \text{ W}/(\text{cm}^2 \text{ cm}^{-1} \text{ sr})$  (Kobayashi et al., 1999). However, the level of noise varies strongly with spectral bands and latitudes. In order to constrain the retrievals, a value of  $\sigma_\varepsilon$  close to the best Root Mean Squares (RMS) has been set (Fig. 1).

Water vapour absorbs all over the spectral domain of IMG, but many strong absorption lines (Clerbaux et al., 2003) overlap and/or saturate the absorption. On this basis, we have selected one spectral window within band 3 for the retrieval of HDO, extending from 1205.40 to 1227.50  $\text{cm}^{-1}$ , and two windows within band 2 for the retrieval of  $\text{H}_2^{18}\text{O}$ , extending respectively from 2004.00 to 2015.32 and 2019.6

to 2032.00  $\text{cm}^{-1}$ . Figure 1 gives a typical example of spectral fit in the selected windows. The fit is good in both bands, with the residual spectra (Observed-Calculated) being close to the expected instrumental noise value.

The VMR for the different water isotopologues are retrieved on 10 vertical levels, in the middle of layers extending from the ground to 20 km as follow : 0–1, 1–3, 3–5, 5–7, 7–9, 9–11, 11–13, 13–15, 15–17 and 17–20 km. In the spectral range used,  $\text{CH}_4$ ,  $\text{H}_2^{17}\text{O}$  and  $\text{CO}_2$  profiles are fixed to standard values. The surface Temperature ( $T_s$ ) and the profiles of  $\text{H}_2^{16}\text{O}$ , HDO and  $\text{H}_2^{18}\text{O}$  are adjusted simultaneously.

## 3 Retrievals and characterizations

### 3.1 Comparison with sondes

This section aims to give insight onto the capabilities of the IMG measurements for determining the vertical profiles of  $\text{H}_2^{16}\text{O}$ , HDO and  $\text{H}_2^{18}\text{O}$  in the troposphere, rather than to perform a quantitative validation of the results. However, in order to ensure that the large scale features of the water distribution on the horizontal and vertical dimensions are well reproduced, we have chosen to compare the retrieved profiles to a restricted set of correlative humidity soundings representative of different latitudes. The latter have been selected from regular balloon launches performed by the Network for the Detection of Atmospheric Composition Change (NDACC) and the World Ozone and Ultraviolet Data Center (WOUDC) in the time period of interest. A set of spectra within  $3^\circ$  latitude/longitude of the eight NDACC or WOUDC

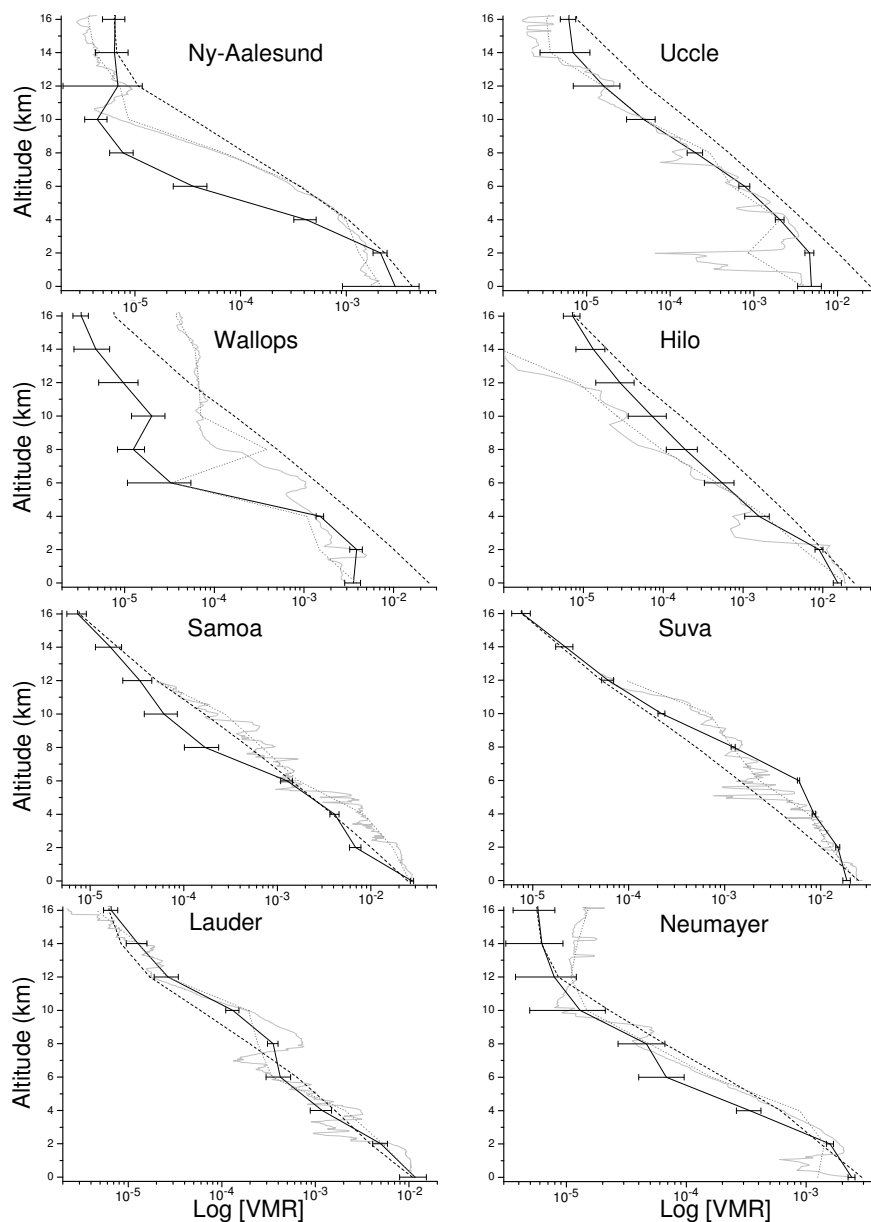


**Fig. 2.** Retrieved water vapour profiles (VMR) up to 16 km from IMG observations between 1 and 10 April 1997 for eight different sites compared with water vapour sonde measurements (see Table 1). The retrieved values are indicated by black lines, the a priori profiles by black dashes, the sonde profiles by grey lines and the smoothed sonde profiles by grey dots.

stations and measured within one day of the soundings has been considered (Table 1). Since the sonde measurements are performed at a very high vertical resolution, they need to be smoothed in order to account for the lower resolution of the IMG observing system and thus to allow a meaningful comparison with the retrieved profiles. The smoothed water vapour sonde profiles  $\mathbf{x}_s$  are calculated from the measured profiles  $\mathbf{x}_{\text{sonde}}$  according to (Rodgers, 2000):

$$\mathbf{x}_s = \mathbf{x}_a + \mathbf{A}(\mathbf{x}_{\text{sonde}} - \mathbf{x}_a) \quad (11)$$

Figure 2 shows the comparisons for each coincident IMG/sonde measurement. In all cases, the retrieved profiles are in fair agreement with the sonde measurements over the entire altitude range covered (0–16 km). Although not shown in Fig. 2, it is interesting to point out that the retrieved  $\text{H}_2^{16}\text{O}$  profiles from band 2 are very similar to those retrieved from band 3, the discrepancies for each layer being less than their respective uncertainty.

In light of Fig. 2, we can safely conclude that the retrievals provide a good representation of the general shape

**Table 1.** Summary of the coincident IMG and water vapour sonde measurements.

Observing Site	Sonde: Latitude, Longitude, Altitude	Day (April 1997) and Time of Sonde measurement (UTC)	IMG: Latitude, Longitude	Day (April 1997) and Time of IMG measurement (UTC)
Ny-Aalesund	78.93°, 11.95°, 11 m	10, 5 h 49 m	79.62°, 11.87°	10, 13 h 39 m
Uccle	50.80°, 4.35°, 100 m	07, 10 h 18 m	51.12°, 6.23°	07, 21 h 32 m
Wallops	37.84°, -75.48°, 13 m	09, 14 h 57 m	35.74°, -73.83°	09, 16 h 01 m
Hilo	19.72°, -155.08°, 11 m	09, 18 h 38 m	21.83°, -154.12°	09, 8h44m
Samoa	-14.23°, -170.56°, 82 m	04, 13 h 42 m	-10.27°, -169.11°	04, 21 h 51 m
Suva	-18.10°, 178.20°, 6 m	04, 22h00m	-18.37°, 174.64°	04, 11 h 15 m
Lauder	-45.04°, 169.68°, 370 m	02, 01h58m	-44.86°, 168.13°	02, 22 h 55 m
Neumayer	-70.65°, -8.26°, 42 m	05, 15 h 18 m	-67.59°, -9.13°	05, 09 h 55 m

of the water vapour profile in the troposphere. In particular, they reproduce adequately the large latitudinal variations but also the altitude gradients up to the tropopause. For tropical scenes (Hilo, Samoa and Suva), the volume mixing ratio is almost one order of magnitude greater than in the highest latitudes and the variation with altitude is important, since more than 90% of the water vapour amount is found between the ground and 6 km. Furthermore, the comparison between the retrieved profiles and the local sonde measurements does not reveal any systematic discrepancy or any dependency with the water vapour amount. The disagreement between the satellite derived values and the sonde data is largest above 4 km, probably as a result of the coincidence criterion, which is loose considering the fast spatial and temporal variation of the water vapour amount (see Table 1). In spite of this, the comparisons highlight the ability of the thermal infrared nadir measurements to provide vertically resolved profiles of water vapour over the entire altitude range of the troposphere, possibly up to the UT/LS region.

The high sensitivity of the IMG measurements to the  $\text{H}_2^{16}\text{O}$  vertical distribution, and to a lower extent to that of the heavier isotopologues, is further illustrated in Fig. 3, for a case corresponding to a high DOFS. Figure 3a shows the retrieved profiles, starting from an a priori profile for the heavier isotopologues ( $\text{H}_2^{18}\text{O}$ , HDO) which is the same as the principal one ( $\text{H}_2^{16}\text{O}$ ), but divided by their respective SMOW ratio. It is seen that the retrieved profiles exhibit similar structures. These profiles do not allow, as such, the detection of any unexpected evolution in the isotopologic vertical distribution.

The averaging kernels associated with these retrievals are shown on Fig. 3b. The measurements are sensitive to  $\text{H}_2^{16}\text{O}$  up to 12 km in altitude and to HDO and  $\text{H}_2^{18}\text{O}$  up to 10 km. The case shown here, is characterized by a DOFS of 5.0 for  $\text{H}_2^{16}\text{O}$ , 2.6 for HDO and 2.3 for  $\text{H}_2^{18}\text{O}$ . The information on the isotopologic ratios, which will be discussed next, is obviously limited by the lowest information content, here HDO and  $\text{H}_2^{18}\text{O}$ .

For each isotopologue, the error budget as a function of altitude is displayed in Fig. 3c. The different curves correspond to the square root of the diagonal elements of the error covariance matrices calculated according to Eqs. (7) to (10). The error analysis confirms that the retrievals are mainly driven by a priori information above 16 km for all isotopologic species. For  $\text{H}_2^{16}\text{O}$ , the principal contributing errors are the smoothing and the measurement errors. For the heavier isotopologues the smoothing error is dominant. Additional contributions ( $\mathbf{S}_{\text{mod,param.}}$ ) to the total retrieval error, including the simultaneous retrievals of the surface temperature and interfering species, are found to be very weak (less than 2%). The total error is particularly small near the surface, where the sensitivity is maximum, with errors reaching 6% for  $\text{H}_2^{16}\text{O}$ , 14% and 12% for HDO and  $\text{H}_2^{18}\text{O}$  respectively. The total errors are smaller than 20% for  $\text{H}_2^{16}\text{O}$ , and than 30% for the heavier isotopologues throughout the troposphere, which is a substantial improvement with respect to the a priori variability. The most significant improvement is located in the troposphere around 6 km, where the a priori uncertainty is 90 %.

The present analysis of the information content shows similarities with the results previously obtained from IMG by Zakharov et al. (2004) for tropospheric  $\text{H}_2^{16}\text{O}$  and from TES by Worden et al. (2006, 2007) for HDO. We find, however, a higher vertical sensitivity to the water isotopologues than in these earlier works. This is very likely due to the softer constraint considered in the present study, where the a priori covariance is much larger than that assumed by Zakharov et al. (2004) and Worden et al. (2006, 2007). In the latter study, the authors estimated the correlation between  $\text{H}_2^{16}\text{O}$  and HDO using a climate model and developed an a priori covariance for the retrievals of the HDO/ $\text{H}_2^{16}\text{O}$  ratio. The retrievals, in our case, are carried out without a priori correlation between the different isotopologues, but the adjustment is performed simultaneously for  $\text{H}_2^{16}\text{O}$  and HDO from band 3 and for  $\text{H}_2^{16}\text{O}$  and  $\text{H}_2^{18}\text{O}$  from band 2.

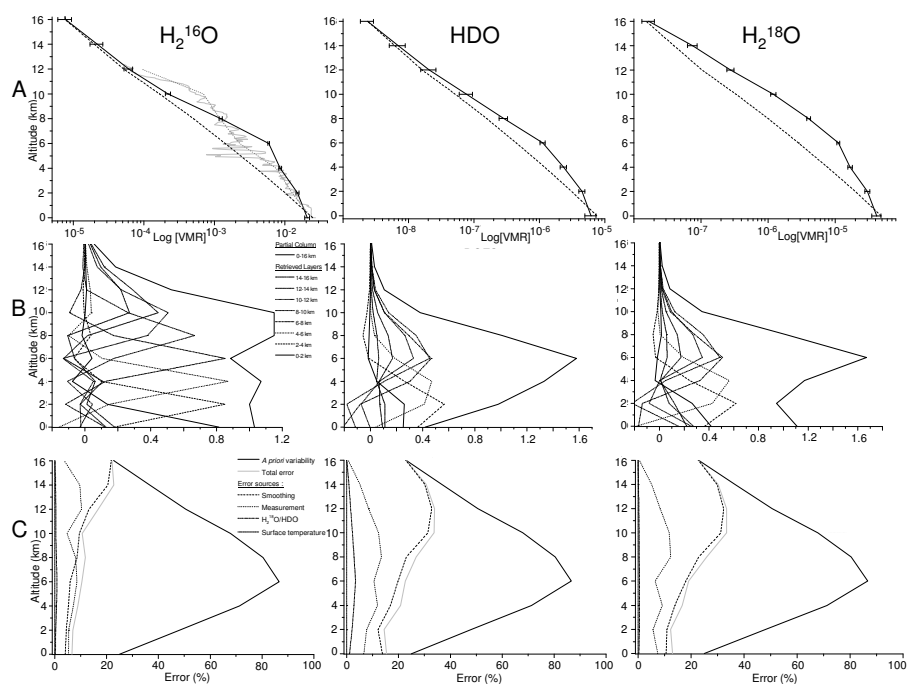


**Fig. 3.** Example of results obtained for a typical scene corresponding to tropical latitudes. **(A)** Retrieved H<sub>2</sub><sup>16</sup>O, H<sub>2</sub><sup>18</sup>O and HDO profiles in VMR units and comparison with a water vapour sonde measurement at Suva. The grey and black lines represent the sonde and retrieved profiles respectively. The grey dots are the smoothed sonde and the black dashes are the a priori profiles. The a priori profiles for H<sub>2</sub><sup>18</sup>O and HDO were taken to be the same as H<sub>2</sub><sup>16</sup>O multiplied by the standard isotopologic ratios. **(B)** Averaging kernels, in volume mixing ratio units, for the three isotopologues. The averaging kernels for the eight retrieved layers are shown, as well as those for the 0–16 km (black lines) columns, representative of the vertical information contained in the measurements. Degrees of freedom for signal are respectively 5, 2.6 and 2.3 for H<sub>2</sub><sup>16</sup>O, HDO and H<sub>2</sub><sup>18</sup>O. **(C)** Error profiles. The curves are the square root of the diagonal elements of the prior and posterior error covariance matrices (Eq. 7 to 10). For computing the errors due to the temperature profiles, uncorrelated uncertainty of 5 K is assumed. The errors due to the uncertainties on the others species (i.e. H<sub>2</sub><sup>17</sup>O, CH<sub>4</sub>, CO<sub>2</sub>) are negligible and therefore not shown.

### 3.2 Isotopologic composition of water vapour

Depletion of heavier water isotopologues relative to the SMOW is measured in parts per mil using the conventional  $\delta$  notation. It is defined as:

$$\delta = \left( \frac{R}{R_{\text{SMOW}}} - 1 \right) \times 1000 \quad (12)$$

Where  $R$  denotes the isotopologic mass ratio, i.e. H<sub>2</sub><sup>18</sup>O/H<sub>2</sub><sup>16</sup>O = 2.0052 · 10<sup>-3</sup> and HDO/H<sub>2</sub><sup>16</sup>O = 0.31152 · 10<sup>-3</sup>. The major source of atmospheric water vapour is the ocean. It is characterized by a SMOW isotopologic composition ( $\delta = 0\%$ ). As explained in the introduction, isotopologically heavier molecules have lower vapour pressure than the main isotopologue, leading to isotopologic fractionation between the phases during condensation and evaporation processes. The fractionation associated with the equilibrium exchange reaction can be expressed using the isotopologue fractionation factor  $\alpha$ :

$$\alpha = R_C / R_V \quad (13)$$

where  $R_C$  and  $R_V$  are the isotopologue ratios of the condensed and vapour phases, respectively. The magnitude of

$\alpha$  depends on many factors, the most important of which is temperature. This fractionation leads to the typical values of  $\delta^{18}\text{O} = -12\%$  and  $\delta D = -85\%$  just above the ocean (Bechtel and Zahn, 2003). When saturated air is lofted and cooled, the heavier isotopologues, which condense more readily, are removed and the isotopologic ratios decrease with altitude. As a consequence,  $R_V$  of the remaining vapour decreases monotonically. In the thermodynamic equilibrium approximation,  $R_V$  is described by the Rayleigh equation:

$$R_V = R_0 f^{(\alpha-1)} \quad (14)$$

Where  $R_0$  is the initial isotopologic ratio in the liquid water,  $f$  is the remaining vapour fraction and  $\alpha$  is the equilibrium fractionation factor during evaporation.

The composition of water isotopologues is affected by complex meteorological processes that provide a characteristic fingerprint of their origin.

In addition to the phase changes under equilibrium conditions, the kinetic effect resulting from a different diffusivity for each isotopologue can be taken into account. The higher diffusivity of HDO, compared to H<sub>2</sub><sup>18</sup>O, results in an additional separation. This partitioning is now recognized as a

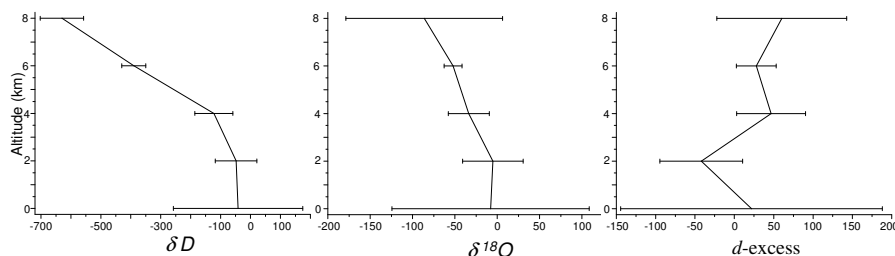


**Fig. 4.** Example of  $\delta D$ ,  $\delta^{18}O$  isotopologic ratios and  $d$ -excess vertical profiles between ground and 8 km of altitude at Suva.

tool for characterizing groundwater from different environments, and is described by the Meteoric Water Line (Bowen and Revenaugh, 2003; Coffey et al., 2006; Bechtel and Zahn, 2003):

$$\delta D = 8\delta^{18}O + 10\text{‰} \text{ (SMOW)} \quad (15)$$

The concept of the deuterium excess is then defined from Eq. (15) as:  $d = \delta D - 8\delta^{18}O$ . Climatic information about the conditions of temperature and humidity prevailing at the evaporative source of the vapour can be inferred from the study of  $d$ .

In light of the averaging kernels and error budgets of Fig. 3, we have restricted the study of the isotopologues depletion to altitudes ranging between 0 and 8 km (see Fig. 4 for the retrieval at Suva). The  $\delta D$ ,  $\delta^{18}O$  and  $d$ -excess calculated from Eq. (12) are obtained using the  $H_2^{16}O$ , HDO and  $H_2^{18}O$  VMR values retrieved independently (i.e. without correlations between the isotopologic species) and the uncertainties are calculated by the standard partial derivatives formula. Thus, the errors that we obtain are largely overestimated as correlations are neglected. The  $\delta D$  and  $\delta^{18}O$  vertical distributions in Fig. 4 exhibit the expected general decay with altitude. The  $\delta$  values and their uncertainties are consistent with those reported in the literature, with different experimental techniques (Gettelman and Webster, 2005; Ehhalt et al., 2005) and  $\delta D$  profile, in particular, can be compared with the results obtained from TES by Worden et al. (2006) between 850 and 300 hPa with a sensitivity peak at around 700 hPa.

Few previous studies have reported  $d$ -excess values (Armengaud et al., 1998; Masson-delmotte et al., 2005; Bowen and Revenaugh, 2003), essentially because it is calculated from very weak variations of the values, so that it needs high sensitivity instruments. For the example of Fig. 4, the uncertainty on the calculation of the  $d$ -excess are very important and even encompass the mean value (i.e. 10‰), which points towards the limitations of the retrievals for the analyses of this quantity. Nevertheless, it is worth pointing out that the negative value at 2 km is correlated with an important increase of the Relative Humidity (96.61%), which is consistent with studies by Bowen and Revenaugh (2003). Additional averaging will, however, be needed to confirm this

result because of the uncertainties in this single profile. It would be interesting to use the  $d$ -excess values on the global scale to improve our understanding of the regional diversity, but since HDO and  $H_2^{18}O$  are retrieved from different scenes on the ground, this can not be undertaken here.

#### 4 Global distributions

For global distribution mapping, only cloud free spectra were selected, using adequate filtering in bands 2 and 3 (Hadji-Lazaro, et al., 2001; Wespes, et al., 2007). Moreover, a filtering based on the spectral root mean square value after retrieval allows discarding excessively noisy spectra. All the global distributions presented here are averaged on a  $5^\circ$  latitude by  $10^\circ$  longitude grid.

Figure 5 shows the global distributions of the DOFS for  $H_2^{16}O$ ,  $H_2^{18}O$  and HDO. As discussed in previous studies (Barret, et al., 2005; Coheur, et al., 2005), a latitudinal dependency of the DOFS, which follows the temperature variations, is observed. High DOFS are found in the tropics, where high surface temperature leads to a higher signal. On the opposite, high latitude regions have lower surface temperature and low DOFS. The effect is mostly pronounced for the heavier isotopologues, whose evaporation is more strongly correlated to temperature. For this reason, the measurements polewards of  $60^\circ$  latitude have been rejected. In-between these limits, the DOFS ranges from 1 to 5 with a mean value of 3 (see Fig. 5) for  $H_2^{16}O$ . The difference between the DOFS distribution pattern of HDO and  $H_2^{18}O$  is linked to the better signal-to-noise ratio achieved in band 3 where HDO is retrieved.

In order to avoid discussing results which depend upon the vertical sensitivity of the measurements to the different isotopologues, we focus hereafter on the global distributions of tropospheric  $H_2^{16}O$ ,  $H_2^{18}O$  and HDO, expressed as a column between 0 and 16 km. They are presented in Fig. 6, along with the latitudinal averaged distributions of the profiles. The measured partial columns range are from about  $0.04$  to  $0.4 \times 10^{24}$ ,  $0.08$  to  $0.8 \times 10^{21}$  and  $0.1$  to  $1.2 \times 10^{20}$  molecules. $\text{cm}^{-2}$  for  $H_2^{16}O$ ,  $H_2^{18}O$  and HDO, respectively. Higher abundances are found within the inter-tropical belt, as can be clearly seen on the latitudinal distributions, with

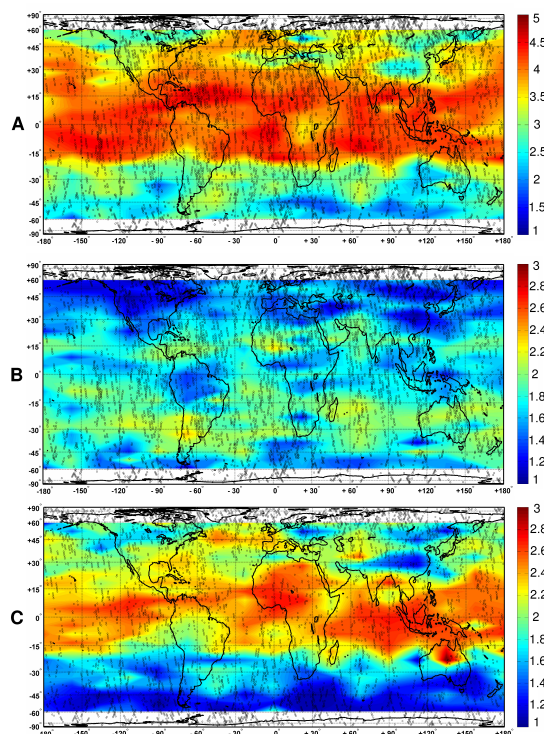


**Fig. 5.** Global distribution of the DOFS. From top to bottom, H<sub>2</sub><sup>16</sup>O (A), H<sub>2</sub><sup>18</sup>O (B) and HDO (C), averaged on a 10° × 5° longitude-latitude grid, for the 1–10 April 1997 period. The black circles show the location of the IMG retrievals

strong impact of surface temperatures and tropopause altitudes on the retrieved profiles. Globally, the water amounts are larger in southern hemisphere, but some local exceptions are visible. For instance, at 40° N, a peak of concentration is observed for H<sub>2</sub><sup>16</sup>O and H<sub>2</sub><sup>18</sup>O. Despite the limited vertical sensitivity of the measurements, large latitudinal and regional variability are also observed, which are most probably linked to a mixing of various air masses.

On the zonal distribution maps, we can see that the H<sub>2</sub><sup>16</sup>O and H<sub>2</sub><sup>18</sup>O concentrations over tropical Continents are larger than those over Oceans, in particular above Amazonia and central Africa. The Ocean–Continent contrast is weaker for HDO, for which only latitudinal variations are observed, due to the progressive atmospheric depletion during poleward transport and precipitation. The latter observation is consistent with HDO global distribution made from the TES instrument.

The distributions of the isotopologic ratios, given in Fig. 7, show a wide range of isotopologic depletion values:  $\delta D$  is indeed between 0 and –800 ‰, while  $\delta^{18}\text{O}$  ranges between 0 and –150‰. The latitudinal distribution also reveals a very large variability of both  $\delta$  values with altitude in the tro-

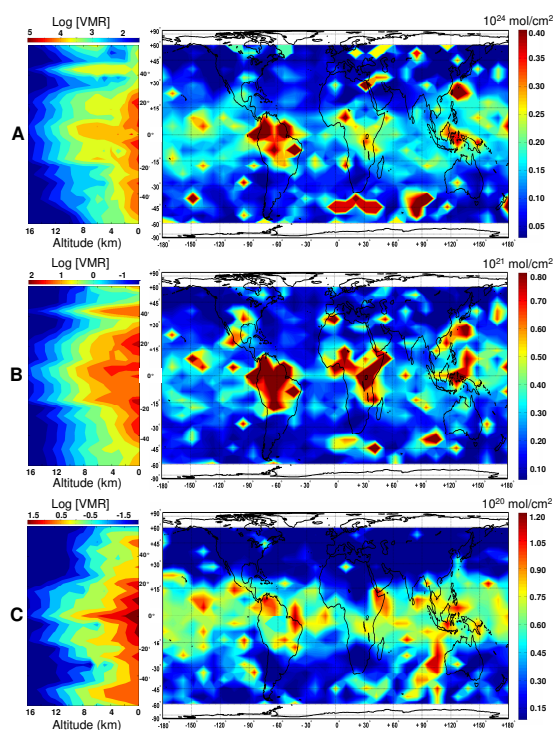


**Fig. 6.** Global distribution of water vapour isotopologues. Latitudinal distributions (left) and zonal distributions (right) of each isotopologue between 0 and 16 km of altitude. The H<sub>2</sub><sup>16</sup>O (A), H<sub>2</sub><sup>18</sup>O (B) and HDO (C) tropospheric columns (0–16 km) are in 10<sup>24</sup>, 10<sup>21</sup> and 10<sup>20</sup> molecules.cm<sup>-2</sup>, respectively. Only profiles with a DOFS larger than 1 are considered. Data are averaged on a 10° × 5° longitude-latitude grid, for the 1–10 April 1997 period.

posphere, consistent with the observation of Webster and Heymsfeld (2003). The less depleted values of  $\delta^{18}\text{O}$  and  $\delta D$  are principally found into the tropics (+20°; –20°). At these latitudes, the maximum values of  $\delta D$  are located between the ground and 2 km and they are quasi-constant above 10 km (see Fig. 7a) as suggested by previous work (Kuang et al., 2003). However, further geophysical analyses of the upper tropospheric values are hindered by the limited sensitivity of the measurements to the heavier isotopologues above 10 km (see Fig. 3).

The zonal mean distributions of the tropospheric columns highlight remarkable regions where  $\delta^{18}\text{O}$  decreases. This is the case, for instance, for Northern America and Eastern Europe (see Fig. 7a). On the opposite, lower depletions are found over the Amazonian Basin and Equatorial Africa. The most apparent trend for  $\delta D$  is the progressive evolution with latitude (see Fig. 7b). However, for both  $\delta^{18}\text{O}$  and  $\delta D$ , several smaller-scale deviations to the general trend are observed. Again, an accurate explanation of these features is



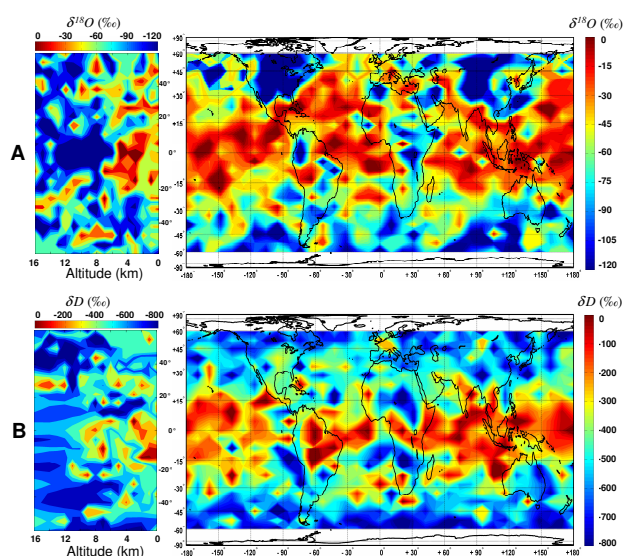


**Fig. 7.** Global distribution of isotopologic ratios. Latitudinal distributions (left) and zonal distributions (right) of  $\delta^{18}\text{O}$  (**A**) and  $\delta D$  (**B**) between 2 and 16 km of altitude. Data are averaged on a  $10^\circ \times 5^\circ$  longitude-latitude grid, for the 1–10 April 1997 period.

difficult, considering the limited vertical sensitivity of measurements and especially its spatial variations. As a matter of consequence, the analyses of the small-scale variations observed on the distributions can hardly be performed with confidence. Globally, however, the results presented here show the potential of high-resolution nadir spectra to study isotopologic composition of tropospheric water vapour on the horizontal and vertical scales and hence provide information about the water cycle on a large scale.

## 5 Conclusions

A set of high-resolution Fourier transform nadir spectra measured by the IMG instrument between 1 and 10 April 1997 has been used to obtain quasi-global distributions of three isotopologic species of water vapour (i.e.  $\text{H}_2^{16}\text{O}$ ,  $\text{H}_2^{18}\text{O}$  and HDO) in the troposphere. For  $\text{H}_2^{18}\text{O}$  these are the first reported global distributions. The retrievals were made using a software relying on the OEM allowing to measure volume mixing ratios and partial columns from the ground up to 16 km.

The comparison of the retrieved profiles with coincident sonde measurements, performed at a series of representative latitudes, has revealed the potential of the satellite measurements to capture the large spatial variations of the water vapour amount in the troposphere. The characterization of the profiles showed that the measurements contain up to 5, 2.6 and 2.3 independent pieces of information on the  $\text{H}_2^{16}\text{O}$ , HDO and  $\text{H}_2^{18}\text{O}$  vertical distributions, respectively. On the basis of the errors and averaging kernels analyses, it was

found that the sensitivity was maximal between the ground and 12 km for  $\text{H}_2^{16}\text{O}$  and between the ground and 8 km for the others isotopologic species. The uncertainties on the tropospheric profiles are less than 20% for the principal isotopologue and 30% for the others, improving significantly the *prior* knowledge. On a case study, we were able to show that the calculated  $\delta D$ ,  $\delta^{18}\text{O}$  and *d*-excess vertical distributions exhibit the expected trends with altitude.

The  $\text{H}_2^{16}\text{O}$ ,  $\text{H}_2^{18}\text{O}$  and HDO zonal and latitudinal distributions, expressed as partial columns in the troposphere, have been presented. The latitudinal distributions reproduce the variation of the tropopause height and also highlight the impact of surface temperature on the water vapour amount. Some Ocean-Continent differences and altitude-dependent variations were also observed and discussed. The global distributions of isotopologic ratios revealed that the depletion of heavier water vapour isotopologues is stronger at higher latitudes. Regional variations have also been observed, but the large uncertainties on the retrieved quantities and the low vertical sensitivity have prevented their geophysical analysis.

Globally, the results have demonstrated the ability of infrared spectroscopy from space to study many tropospheric processes for which water vapour and isotopologues play a significant role from the local to the global scale. The results open promising perspectives for future space missions. This will be the case for the Infrared Atmospheric Sounding Interferometer (IASI) onboard MetOp platforms (Clerbaux et al., 2007) whose data are expected to improve our understanding of the chemistry, transport and climate.

*Acknowledgements.* The research was funded by the Fonds National de la Recherche Scientifique (FNRS, Belgium), the Belgian State Federal Office for Scientific, Technical and Cultural Affairs and the European Space Agency (ESA-Prodex arrangement C90-220). Financial support by the “Actions de Recherche Concertées” (Communauté Française de Belgique) is also acknowledged. This work was undertaken in the framework of the ISSWG (IASI Sounding Science Working Group) activities under the auspices of EUMETSAT (European Organization for the Exploitation of Meteorological Satellites) and CNES (Centre National d’Etudes Spatiales). The authors are grateful to IMGDIS/ERSDAC for providing the IMG level 1 data. ECMWF ERA-40 data used in this study have been obtained from the ECMWF data server. Several data used in this publication were obtained as part of the Network for the Detection of Atmospheric Composition Change (NDACC) and the World Ozone and Ultraviolet Radiation Data Centre (WOUDC) and are publicly available (see <http://www.ndsc.ncep.noaa.gov>, <http://www.woudc.org/>).

Edited by: R. Cohen

## References

Armengaud, A., Koster, R. D., Jouzel, J., and Ciais, P.: Deuterium excess in Greenland snow: Analysis with sim-



- ple and complex models, *J. Geophys. Res.*, 103(D8), 8947, doi:10.1029/98JD00274, 1998.
- Barret, B., Turquety, S., Hurtmans, D., Clerbaux, C., Hadji-Lazaro, J., Bey, I., Auvray, M., and Coheur, P.-F.: Global carbon monoxide vertical distributions from spaceborne high-resolution FTIR nadir measurements, *Atmos. Chem. Phys.*, 5, 2901–2914, 2005, <http://www.atmos-chem-phys.net/5/2901/2005/>.
- Bechtel, C. and Zahn, A.: The isotopologue composition of water vapour: A powerful tool to study transport and chemistry of middle atmospheric water vapour, *Atmos. Chem. Phys. Discuss.*, 3, 3991–4036, 2003, <http://www.atmos-chem-phys-discuss.net/3/3991/2003/>.
- Bowen, G. J. and Revenaugh, J.: Interpolating the isotopologic composition of modern meteoric precipitation, *Water Resour. Res.*, 39(10), 1299, doi:10.1029/2003WR002086, 2003.
- Ciais, P. and Jouzel, J.: Deuterium and oxygen 18 in precipitation: Isotopologic model, including mixed cloud processes, *J. Geophys. Res.*, 99(D8), 16793, doi:10.1029/94JD00412, 1994.
- Clerbaux, C., Hadji-Lazaro, J., Turquety, S., Mégie, G., and Coheur, P.-F.: Trace gas measurements from infrared satellite for chemistry and climate applications, *Atmos. Chem. Phys.*, 3, 1495–1508, 2003, <http://www.atmos-chem-phys.net/3/1495/2003/>.
- Clerbaux, C., Hadji-Lazaro, J., Turquety, S., George, M., Coheur, P.-F., Hurtmans, D., Wespes, C., Herbin, H., Blumstein, D., Tournier, B., and Phulpin, T.: The IASI/MetOp mission: first observations and highlight of its potential contribution to the GMES Earth observation component, *Space Res. Today*, 168, 19–24, 2007.
- Clough, S. A., Shephard, M. W., Mlawer, E., Delamere, J. S., Iacono M., Cady-Pereira, K., Boukabara, S., and Brown, P. D.: Atmospheric radiative transfer modeling: A summary of the AER codes, *J. Quant. Spectrosc. Radiat. Transf.*, 91, 233–244, 2005.
- Coffey, M. T., Hannigan, J. W., and Goldman, A.: Observations of upper tropospheric/lower stratospheric water vapour and its isotopologues, *J. Geophys. Res.*, 111(D14), doi:10.1029/2005JD006093, 2006.
- Coheur, P.-F., Barret, B., Turquety, S., Hurtmans, D., Hadji-Lazaro, J., and Clerbaux, C.: Retrieval and characterization of ozone vertical profiles from a thermal infrared nadir sounder, *J. Geophys. Res.*, 110(D24), doi:10.1029/2005JD005845, 2005.
- Ehhalt, D. H., Rohrer, F., and Fried, A.: Vertical profiles of HDO/H<sub>2</sub>O in the troposphere, *J. Geophys. Res.*, 110(D13), doi:10.1029/2004JD005569, 2005.
- Forster, P. M. D. and Shine, K. P.: Assessing the climate impact of trends in stratospheric water vapour, *Geophys. Res. Lett.*, 29(6), 1086, doi:10.1029/2001GL013909, 2002.
- Franz, P. and Rockmann, T.: High-precision isotopologue measurements of H<sub>2</sub><sup>16</sup>O, H<sub>2</sub><sup>17</sup>O, H<sub>2</sub><sup>18</sup>O, and the Δ<sup>17</sup>O-anomaly of water vapour in the southern lowermost stratosphere, *Atmos. Chem. Phys.*, 5, 2949–2959, 2005, <http://www.atmos-chem-phys.net/5/2949/2005/>.
- Gat, J. R. and Matsui, E.: Atmospheric water balance in the Amazon basin: an isotopic evapotranspiration model, *J. Geophys. Res.*, 96, 13 179–13 188, 1991.
- Gedzelman, S., Hindman, E., Zhang, X., Lawrence, J., Gamache, J., Black, M., Black, R., Dunion, J., and Willoughby, H.: Probing Hurricanes with stable isotopologues of rain and water vapour, *Mon. Weather Rev.*, 131, 1112–1127, 2003.
- Gettelman, A. and Webster, C. R.: Simulations of water isotopologue abundances in the upper troposphere and lower stratosphere and implications for stratosphere troposphere exchange, *J. Geophys. Res.*, 110(D17), doi:10.1029/2004JD004812, 2005.
- Hadji-Lazaro, J., Clerbaux, C., Couvert, P., Chazette, P., and Boone, C.: Cloud filter for CO retrieval from IMG infrared spectra using ECMWF temperatures and POLDER cloud data, *Geophys. Res. Lett.*, 28(12), 2397, doi:10.1029/2000GL012342, 2001.
- Hanisco, T. F., Moyer, E. J., Weinstock, E. M., St. Clair, J. M., Sayres, D. S., Smith, J. B., Lockwood, R., and Anderson J. G.: Observations of deep convective influence on stratospheric water vapor and its isotopic composition, *Geophys. Res. Lett.*, 34, L04814, doi:10.1029/2006GL027899, 2007.
- Hartmann, D. L.: Climate Change : Tropical Surprises, *Science*, 295, 811–812, 2002.
- Jouzel, J., Alley, R. B., Cuffey, K. M., Dansgaard, W., Grootes, P., Hoffmann, G., Johnsen, S. J., Koster, R. D., Peel, D., Shuman, C. A., Stievenard, M., Stuiver, M., and White, J.: Validity of the temperature reconstruction from water isotopologues in ice cores, *J. Geophys. Res.*, 102(C12), 26471, doi:10.1029/97JC01283, 1997.
- Keith, D. W.: Stratosphere-troposphere exchange: Inferences from the isotopic composition of water vapor, *J. Geophys. Res.*, 105(D12), 15167, doi:10.1029/2000JD900130, 2000.
- Kirk-Davidoff, D. B., Hints, E. J., Anderson, J. G., and Keith, D. W.: The effect of climate change on ozone depletion through changes in stratospheric water vapour, *Nature*, 402, 399–401, 1999.
- Kobayashi, H., Shimota, A., Kondo, K., Okumura, E., Kameda, Y., Shimoda, H., and Ogawa, T.: Development and evaluation of the interferometric monitor for greenhouse gases: A high-throughput Fourier-transform infrared radiometer for nadir Earth observation, *Appl. Optics*, 38, 6801–6807, 1999.
- Kuang, Z. M., Toon, G. C., Wennberg, P. O., and Yung, Y. L.: Measured HDO/H<sub>2</sub>O ratios across the tropical tropopause, *Geophys. Res. Lett.*, 30(7), 1372, doi:10.1029/2003GL017023, 2003.
- Lawrence, J. R., Gedzelman, S. D., Gamache, J., and Black, M.: Stable isotopologue ratios: Hurricane Olivia, *J. Atmos. Chem.*, 41, 67–82, 2002.
- Lawrence, J. R., Gedzelman, S. D., Dexheimer, D., Cho, H.-K., Carrie, G. D., Gasparini, R., Anderson, C. R., Bowman, K. P., and Biggerstaff, M. I.: Stable isotopic composition of water vapor in the tropics, 109(D06), doi:10.1029/2003JD004046, 2004.
- Masson-Delmotte, V., Jouzel, J., Landais, A., Stievenard, M., Johnsen, S. J., White, J. W. C., Werner, M., Sveinbjornsdottir, A., and Fuhrer, K.: GRIP Deuterium excess reveals rapid and orbital-scale changes in Greenland moisture origin, *Science*, 309, 118–121, 2005.
- McCarthy, M. C., Boering, K. A., Rahn, T., Eiler, J. M., Rice, A. L., Tyler, S. C., Schauffler, S., Atlas, E., and Johnson, D. G.: The hydrogen isotopologic composition of water vapour entering the stratosphere inferred from high-precision measurements of δD-CH<sub>4</sub> and δD-H<sub>2</sub>, *J. Geophys. Res.*, 109(D07), doi:10.1029/2003JD004003, 2004.
- Moyer, E. J., Irion, R. W., Yung, Y. L., and Gunson, M. R.: ATMOS stratospheric deuterated water vapour and implications for troposphere-stratosphere transport, *Geophys. Res. Lett.*, 23(17), 2385, doi:10.1029/96GL01489, 1996.
- Rodgers, C. D.: Inverse Methods for Atmospheric Sounding: The-

- ory and Practice, World Sci., Hackensack, N. J, 2000.
- Rosenlof, K. H., Oltmans, S. J., Kley, D., Russell, J. M., Chiou, E.-W., Chu, W. P., Johnson, D. G., Kelly, K. K., Michelsen, H. A., Nedoluha, G. E., Remsberg, E. E., Toon, G. C., McCormick, M. P.: Stratospheric water vapour increases over the past half-century, *Geophys. Res. Lett.*, 28(7), 1195, doi:10.1029/2000GL012502, 2001.
- Rosenlof, K. H.: How water enters the stratosphere, *Science*, 302, 1691–1692, 2003.
- Rothman, L. S., Jacquemart, D., Barbe, A., Chris Benner, D., Birk, M., Brown, L. R., Carleer, M. R., Chackerian Jr., C., Chance, K., Coudert, L. H., Dana, V., Devi, V. M., Flaud, J.-M., Gamache, R. R., Goldman, A., Hartmann, J.-M., Jucks, K. W., Maki, A. G., Mandin, J.-Y., Massie, S. T., Orphal, J., Perrin, A., Rinsland, C. P., Smith, M. A. H., Tennyson, J., Tolchenov, R. N., Toth, R. A., Vander Auwera, J., Varanasi, P., Wagner G.: The HITRAN 2004 molecular spectroscopic database, *J. Quant. Spectrosc. Radiat. Transf.*, 96, 139–204, 2005.
- Schmidt, G. A., Hoffmann, G., Shindell, D. T., and Hu, Y.: Modelling atmospheric stable water isotopologues and the potential for constraining cloud processes and stratosphere-troposphere water exchange, *J. Geophys. Res.*, 110(D21), doi:10.1029/2005JD005790, 2005.
- Schneider, E. K., Kirtman, B. P., and Lindzen, R. S.: Tropospheric Water Vapour and Climate Sensitivity, *J. Atmos. Sci.*, 56, 1649–1658, 1999.
- Shindell, D. T.: Climate and ozone response to increased stratospheric water vapour, *Geophys. Res. Lett.*, 28(8), 1551, doi:10.1029/1999GL011197, 2001.
- Smith, R.B.: Deuterium in North Atlantic storm tops, *J. Atmos. Sci.*, 49, 2041–2057, 1992.
- Solomon, S.: Stratospheric ozone depletion: A review of concepts and history, *Rev. Geophys.*, 37, 275–316, 1999.
- Strong, M., Scharp, Z. D., and Gutzler, D. S.: Diagnosing moisture transport using D/H ratios of water vapor, *Geophys. Res. Lett.*, 34, L03404, doi:10.1029/2006GL028307, 2007.
- Tabazadeh, A., Santee, M. L., Danilin, M. Y., Pumphrey, H. C., Newman, P. A., Hamill, P. J., and Mergenthaler, J. L.: Quantifying denitrification and its effect on ozone recovery, *Science*, 288, 1407–1411, 2000.
- Webster, C. R. and Heymsfield, A. J.: Water isotopologue ratios D/H,  $^{18}\text{O}/^{16}\text{O}$ ,  $^{17}\text{O}/^{16}\text{O}$  in and out of clouds map dehydration pathways, *Science*, 302, 1742–1745, 2003.
- Wespes, C., Hurtmans, D., Herbin, H., Barret, B., Turquety, S., Hadji Lazaro, J., Clerbaux, C. and Coheur, P.-F.: Satellite measurements of nitric acid global distributions in the troposphere and the stratosphere, *J. Geophys. Res.*, 112, D13311, doi:10.1029/2006JD008202, 2007.
- Worden, J., Bowman, K., Noone, D., Beer, R., Clough, S., Eldering, A., Fisher, B., Goldman, A., Gunson, M., Herman, R., Kulawik, S. S., Lampel, M., Luo, M., Osterman, G., Rinsland, C., Rodgers, C., Sander, S., Shephard, M., and Worden, H.: Tropospheric Emission Spectrometer observations of the tropospheric HDO/H<sub>2</sub>O ratio: Estimation approach and characterization, *J. Geophys. Res.*, 111(D16), doi:10.1029/2005JD006606, 2006.
- Worden, J., Noone, D., Bowman, K., Beer, R., Clough, S., Eldering, A., Fisher, B., Gunson, M., Goldman, A., Herman, R., Kulawik, S. S., Lampel, M., Osterman, G., Rinsland, C., Rodgers, C., Sander, S., Shephard, M., Webster, C. R. and Worden, H.: Importance of rain evaporation and terrestrial sources in the tropical water cycle, *Nature*, 445, 528–532, 2007.
- Zahn, A., Franz, P., Bechtel, C., Groo, J.-U., and Röckmann, T.: Modelling the budget of middle atmospheric water vapour isotopologues, *Atmos. Chem. Phys.*, 6, 2073–2090, 2006, <http://www.atmos-chem-phys.net/6/2073/2006/>.
- Zakharov, V. I., Imasu, R., Griбанov, K. G., Hoffmann, G., and Jouzel, J.: Latitudinal distribution of the deuterium to hydrogen ratio in the atmospheric water vapour retrieved from IMG/ADEOS data, *Geophys. Res. Lett.*, 31, L12104, doi:10.1029/2004GL019433, 2004.